

### **3. LOW PRESSURE-TEMPERATURE EVOLUTION OF THE CONTINENTAL CRUST EXHUMED DURING THE OPENING OF THE WOODLARK BASIN<sup>1</sup>**

Véronique Gardien,<sup>2</sup> Bernard LeGall,<sup>3</sup> Bernard Célérier,<sup>4</sup>  
Véronique Louvel,<sup>5</sup> and Philippe Huchon<sup>6</sup>

#### **ABSTRACT**

During the last 8 m.y. the Papuan Peninsula region of Papua New Guinea has been affected by extension which opened the Woodlark Basin. The present-day spreading tip is located at the foot of the Moresby Seamount, a crustal block whose northern flank is an active low-angle normal fault related to this extension. During Ocean Drilling Program Leg 180 (7 June–11 August 1998), 11 sites (1108–1118) were drilled along a north-south-trending transect across the Woodlark Basin just ahead of the spreading tip. Four of these sites (1118, 1109, 1114, and 1117) reached the crystalline basement, which is composed of diabase and gabbro. Sites 1118 and 1109, located on the Woodlark Rise, belong to the hanging wall block, and Sites 1114 and 1117, located on the crest of the Moresby Seamount, belong to the footwall block and the fault zone itself. Most of the basalt, diabase, and gabbro that were recovered show a well-preserved magmatic texture. The diabase, which is the most abundant rock type, has a coarse-grained ophitic texture composed of poikilitic clinopyroxene including radiating, locally skeletal plagioclase laths with interstitial iron oxide grains. Secondary mineralogy consists of chlorite, zeolite, calcite, albite, and quartz. The gabbro shows a medium-grained granular texture. The magmatic mineralogy consists of euhedral laths of plagioclase and anhedral interstitial clinopyroxene. Secondary mineralogy consists of a magnesio to actinolitic hornblende, chlorite, clinozoisite, zeolite, quartz, and calcite. The retro-

<sup>1</sup>Gardien, V., LeGall, B., Célérier, B., Louvel, V., and Huchon, P., 2002. Low pressure-temperature evolution of the continental crust exhumed during the opening of the Woodlark Basin. *In* Huchon, P., Taylor, B., and Klaus, A. (Eds.), *Proc. ODP, Sci. Results*, 180, 1–28 [Online]. Available from World Wide Web: <[http://www-odp.tamu.edu/publications/180\\_SR/VOLUME/CHAPTERS/178.PDF](http://www-odp.tamu.edu/publications/180_SR/VOLUME/CHAPTERS/178.PDF)>. [Cited YYYY-MM-DD]

<sup>2</sup>Université Lyon1, CNRS UMR 5570, 69622 Villeurbanne, Cedex, France. [vgardien@univ-lyon1.fr](mailto:vgardien@univ-lyon1.fr)

<sup>3</sup>Institut Universitaire Européen de la Mer, CNRS UMR 6538, 29280 Plouzané, France.

<sup>4</sup>ISTEEM, CNRS Université de Montpellier II, cc MSE, 34095 Montpellier Cedex 5, France.

<sup>5</sup>Laboratoire des mesures de Forage, ISTEEM, CNRS Université de Montpellier II, cc 57, 34095 Montpellier Cedex 5, France.

<sup>6</sup>Géosciences Azur, Observatoire océanologique de Villefranche, BP 48, 06235 Villefranche sur Mer, France.

Initial receipt: 25 October 2001

Acceptance: 26 April 2002

Web publication: 31 July 2002

Ms 180SR-178

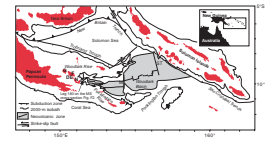
grade metamorphic evolution of both gabbro and diabase occurred under low amphibolite to subgreenschist facies conditions associated mainly with brittle deformation and the development of a local low-temperature shear zone. This shows no evidence for high thermal gradient in the crust during the continental rifting.

## INTRODUCTION

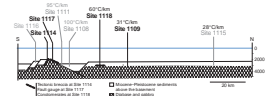
The Woodlark basin is located east of the southeastern tip of the Papuan Peninsula region of Papua New Guinea (Fig. F1). This region is tectonically very active, as it has been affected since the Mesozoic by the oblique convergence between the Australian and the Pacific plates and by present-day subduction zones represented by the Solomon Sea Triple Junction (the New Britain Trench and the Trobriand Trough north and south of the Solomon Sea) and the San Cristobal Trench on the western side of the Solomon Islands. In addition to this complex tectonic setting, the Papuan Peninsula region has been affected by extension for the last 8 m.y., associated with westward-propagating spreading that opened the Woodlark Basin. The present-day spreading tip ( $9^{\circ}45'S$ ,  $151^{\circ}45'E$ ) is situated east of the Moresby Seamount ( $9^{\circ}50'S$ ,  $151^{\circ}35'E$ ), which forms a bathymetric high (12 km long and 7 km wide) oriented northeast-southwest. A low-angle normal fault emerges along the northern flank of the Moresby Seamount. This east-west-oriented active low-angle normal fault (Abers, 1991; Wernicke, 1995; Abers et al., 1997) is related to the present extension occurring in the Woodlark Basin and separates a footwall margin to the south (the Moresby Seamount) and a hanging wall margin to the north (the Woodlark Rise).

During Leg 180 (7 June–11 August 1998) in the Woodlark Basin, 11 sites (1108–1118) were drilled along a north-south-trending transect. Sites 1114, 1116, and 1117, located just on the top of the Moresby Seamount, are part of the footwall margin. Sites 1108 and 1110–1113 at the foot of the Moresby Seamount are located just above the low-angle normal fault. Sites 1118, 1109, and 1115, located on the Woodlark Rise, are part of the hanging wall margin. Four of these sites (1114, 1117, 1118, and 1109) reached the crystalline basement, which is composed mostly of diabase with minor gabbro and basalt (Fig. F2). Two diabase samples from Hole 1109D and one gabbro sample from Site 1117 were dated by the Ar/Ar method (plagioclase and whole rock) and by U/Pb on zircon. The different samples gave ages of  $66.4 \pm 1.5$  Ma, interpreted as the crystallization age (Monteleone et al., this volume), and  $58.9 \pm 5.8$  and 44 Ma, interpreted as cooling ages (Monteleone et al. and Brooks and Tegner, both this volume). This dating indicates that the Moresby Seamount is part of the Papuan ophiolites that belong in the Central Ophiolites belt, which lies from the northwest to the southeastern tip of the Papua New Guinea island. Previous studies suggest that the ophiolites were formed from an oceanic (Johnson and Jaques, 1980; Jenner, 1981; Davies and Jaques, 1984) to a backarc environment (Monnier et al., 2000) accreted during Jurassic to Cretaceous times (Jaques and Chapell, 1980) and obducted onto the Australian margin during the Eocene–Miocene Melanesian orogenesis (Davies and Jaques, 1984). Superimposed on the Paleocene subduction and collision, a middle Miocene to Holocene arc magmatism characterized by abundant andesite, high-K basalt, and peralkaline rhyolite volcanism is represented on the southeast Papuan Peninsula and on the Normanby, Goodenough, and Ferguson Islands (Fig. F1). This volcanism is interpreted as the re-

F1. Regional setting and tectonics of the Papua New Guinea–Solomon Islands region, p. 14.



F2. Schematic cross-section of Leg 180 sites, p. 15.



sult of the present-day slow subduction at the Trobriand Trough (Hamilton 1979; Davies and Jaques, 1984; Lock et al., 1987), though this interpretation remains controversial given the small number of intermediate-depth earthquakes beneath this region (Abers and Roecker, 1991). Since the Pliocene, a north-south extension concentrated between Ferguson and Solomon Islands is responsible for the opening of the Woodlark Basin and propagates westward into the Papuan Peninsula (Taylor et al., 1995). Extension would also be responsible for both the formation of metamorphic core complexes in the D'Entrecasteaux Islands, with the possible participation of magma underplating, and their exhumation by tectonic denudation along ductile extensional shear zones (Baldwin et al., 1993, and references therein).

This study will present petrological data including mineral phase analyses and thermobarometrical calibrations of the basement rocks recovered during Leg 180 (from Sites 1114, 1117, 1118, and 1109), which will be discussed with respect to the present-day very complex tectonic environment.

## SITE CHARACTERISTICS

### Hanging Wall Margin

Sites 1118 and 1109 are located on the Woodlark Rise on the hanging wall margin, 2 and 11 km north, respectively, of the south-dipping normal fault antithetical to the active low-angle normal fault that emerges at the northern flank of the Moresby Seamount.

At Site 1118, 58 m of cored section (average recovery = 22.67%) yielded 13.56 m of mafic rocks. The igneous basement was reached between Sections 180-1118A-70R-3 and 76R-3 at a water depth of 2303.6 m and below 663.7 m of Pliocene limestone, calcareous paraconglomerates, and volcanoclastic sandstone. The whole sedimentary sequence records the progressive subsidence of an early Pliocene subaerially eroded and tropically weathered landmass (see "Lithostratigraphy" in Shipboard Scientific Party, 1999b). In Hole 1109D, mafic rocks were cored below 2211.1 m of water and 735 m of upper Miocene to upper Pleistocene sediments (see "Lithostratigraphy" in Shipboard Scientific Party, 1999a). This igneous material was first present as clasts between 743.9 (Section 180-1109D-43R-1) and 763.2 meters below seafloor (mbsf) (Section 45R-3) in a conglomeratic zone containing well-rounded pebbles of glassy basalt and fine-grained diabases included in a clayey matrix interpreted as fluvial deposits (see "Lithostratigraphy" in Shipboard Scientific Party, 1999a). Below the conglomerate, 34.9 m (average recovery = 65%) of massive mafic rocks was cored between 770 (Section 180-1109D-45R-4) and 802 (Section 51R-4) mbsf.

### Footwall Margin

Sites 1117 and 1114, separated by 3.5 km, are located on the upper slope of the northern flank and on the crest of the Moresby Seamount, respectively.

At Site 1117, recovery averaged 5.1% and only 6.57 m of mafic rock was recovered below 1163 m of water. The hole began in a soft, light-colored clayey material interpreted as a fault gouge. Shipboard X-ray analyses indicate a mixture of talc, chlorite, calcite, ankerite, and serpentine (chrysotile, lizardite, and antigorite). True cohesive metamor-

phic rocks were recovered at 57 mbsf. Relatively fresh quartz gabbro was recovered with grain sizes up to 8 mm and a hypidiomorphic texture at 85 mbsf (Core 180-1117A-11R).

At Site 1114, 67 m of igneous mafic rocks was recovered below 286 m of Pliocene–Pleistocene sediments (below the sediment, average recovery = 13%). The igneous mafic rocks were first recovered in a tectonic breccia (Section 180-1114A-31R-1) overlying the massive mafic rocks cored between Cores 180-1114A-32R (295.5 mbsf) and 37R (345.5 mbsf), corresponding to the base of the hole.

## MAGMATIC AND DEFORMATIONAL TEXTURE

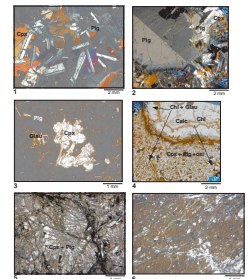
### Hanging Wall Margin

In Hole 1109D, two types of igneous mafic rocks were recovered, undeformed metamorphosed basalt and diabase. Most of the cored igneous rocks display a well-preserved magmatic texture. The diabases that are the most abundant rock type display a coarse-grained ophitic texture composed of poikilitic clinopyroxene including radiating, locally skeletal plagioclase laths, 1 to 2 mm long, with interstitial iron oxide grains (Pl. P1, fig. 1). The grain size of the minerals increases from top (Core 180-1109D-45R) to bottom (Section 50R-3). This is clearly visible for the plagioclase that becomes porphyroclastic up to 5–6 mm in diameter (Pl. P1, fig. 2). From Section 180-1109D-51R-1 to 51R-3, the diabase displays a grain-size reduction until the very bottom of the hole (Section 51R-4), where a basaltic texture is observed (Pl. P1, fig. 3). The basaltic samples are composed of dark brown groundmass with quenched and spherulitic structures. The microlites of plagioclase between the spherulites show split ends. This presence of basaltic levels in the diabase was interpreted as the glassy chilled margin of a second sill injection rapidly cooled at the contact with the previous diabase sill or dyke (see “Igneous and Metamorphic Petrology” in Shipboard Scientific Party, 1999a).

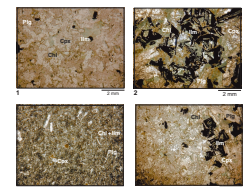
Little evidence of tectonic deformation is recorded in the Hole 1109D diabase. The deformation is illustrated by extensional joints crosscutting the rocks and filled with hydrothermal assemblages composed of zeolite, quartz, chlorite, and calcite (Pl. P1, fig. 4). This is consistent with the almost-continuous unfaulted character of the sedimentary sequence (given by the seismic image) that overlays the basement. Indeed, brittle faulting and fracturing in the sediment is limited to the lower part of the cored section, close to the lithologic boundary between sediments and basement. It suggests that the variation in the lithologic competency was a significant factor in controlling strain. The fault pattern results from extension, assumed to be post-middle Miocene in age (see “Structural Geology” in Shipboard Scientific Party, 1999a), compatible with the Woodlark Basin north-south extension (C  lerier et al., this volume).

At Site 1118, diabase was recovered in Sections 180-1118A-70R-1 to 76R-2 below a conglomeratic unit composed of carbonate matrix containing rounded basaltic clasts (see “Lithostratigraphy” in Shipboard Scientific Party, 1999b). The rocks are slightly to moderately altered and fractured. They are coarse to fine grained, with granular to ophitic texture. Mineralogy includes fresh pyroxene, saussuritised plagioclase often overgrown with dendritic iron oxide, and, less commonly, with pyrite (Pl. P2, fig. 1). Clusters of greenish layer silicates represent

P1. Photomicrographs of diabase, p. 26.



P2. Photomicrographs of diabase, Site 1118, p. 27.



pseudomorphs from olivine. Grain size varies moderately throughout the zone. However, two coarse-grained zones are present at the bottom of the cored section at Samples 180-1118A-74R-2 (Piece 5, 120–149 cm) and 76R-2 (Pieces 11 and 12, 77–89 cm) (Pl. P2, fig. 2). In these intervals, the diabase has a coarse-grained texture and minerals reach 1 to 2 mm in size with spectacular dendritic ilmenite better developed than that observed at Site 1117 (Pl. P2, fig. 2). There is an abrupt change between the granular and the coarse-grained textures (Pl. P2, figs. 2, 3).

The Site 1118 diabase is locally affected by brittle deformation characterized by the development of breccia (Pl. P2, fig. 4). This deformation occurs locally in Sections 180-1118A-71R-1 to 73R-2 (878.4–889.4 mbsf) and 74R-3 to 75R-1 and 75R-2 (900.4–907.1 mbsf). Between the brecciated zones, the diabase is undeformed and preserves a magmatic granular texture. The two brecciated zones are interpreted as fluid circulation zones responsible for the weathering of the rocks (see “Igneous and Metamorphic Petrology” in Shipboard Scientific Party, 1999a).

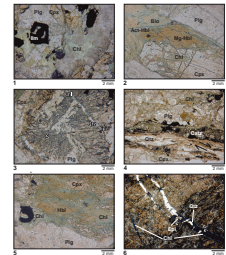
### Footwall Margin

At Site 1117, undeformed to intensely deformed metamorphosed quartz gabbro was recovered. The gabbro shows a medium-grained granular texture (the grain size locally reaches 0.5 to 1 cm). The primary magmatic texture consists of euhedral laths of plagioclase, subhedral interstitial clinopyroxene (Pl. P3, fig. 1), and xenomorph quartz grains forming aggregates. Dendritic ilmenite is observed in some samples, although in general, samples contain skeletal ilmenite and quartz grains. Secondary mineralogy consists of zoned amphibole, chlorite, clinzoisite, zeolite quartz, and calcite. The zoned amphiboles have a brown core and a green to bluish green rim (Pl. P3, fig. 2) that is continuous with green fibrous amphiboles replacing phenocrysts of former clinopyroxene. Few biotites are developed in association with amphiboles (Pl. P3, fig. 2). Zeolite replaces plagioclase, whereas chlorite associated with pale green phrenite needles is present after both pyroxene and amphibole. Chlorite is also present in veins. In the undeformed gabbro, symplectite textures are developed at the contact between plagioclase and clinopyroxene. The symplectite consists of an intergrowth of albite and chlorite lamellae, probably representing a retrogressed association from a former plagioclase and clinopyroxene assemblage (Pl. P3, fig. 3).

The upper cored section (Sections 180-1118A-7R-1 and 9R-1) is characterized by a sheared texture of partially calcitized gabbro. Downhole, two shear zones are observed in intervals 180-1118A-11R-1, 46–55 cm, and 12R-1, 29–34 cm. In the tectonized part of the gabbro, the crushing evolved into localized cataclasite within which a dark brown matrix composed of zeolite, clay minerals, and chlorite, including also small pyroxene, amphibole, and epidote grains, are observed. A ductile shear zone made of recrystallized quartz (<0.2 mm) is present crosscutting the cataclasite (Pl. P3, fig. 4). The microscopic observation shows that during the deformation, the porphyroclastic amphiboles were retrogressed to synkinematic chlorites along their cleavage planes (Pl. P3, fig. 5). This suggests that deformation took place under greenschist facies and low pressure conditions. Successive generations of veins filled with quartz and epidote assemblages, chlorite, or calcite cut the breccia (Pl. P3, fig. 6).

At Site 1114, the rocks recovered consist of intensively deformed and metamorphosed basalt and diabase. Locally, in less deformed zones, an ophitic texture composed of poikilitic clinopyroxene including radiat-

P3. Photomicrographs of diabase, Site 1117, p. 28.



ing plagioclase laths of 1 mm is preserved (Pl. P1, fig. 5). This texture is similar to that observed in the Hole 1109D diabase. Most of the mafic rocks recovered at Site 1114 are intensively brecciated and retrogressed (Pl. P1, fig. 6).

## MINERAL CHEMISTRY

Phase compositions were obtained with a Camebax (SX100) microprobe at Clermont-Ferrand University, using silicate, vanadate, and oxide standards (accelerating voltage = 15 kV; beam current = 20 nA at 1 mm diameter; counting time = 10 s). In the following section we will only consider Sites 1109, 1117, and 1118 because the rocks from Site 1114 are intensively altered and did not allow good mineral analyses.

### Primary Mineralogy

#### Site 1109 Diabase

At Site 1109 the rocks showing basaltic texture (Sample 180-1109D-41R-3, 72–74 cm) are composed of augitic clinopyroxene ( $\text{Wo}_{40}\text{En}_{46-50}\text{Fs}_{10-12}$ ) displaying low Ti content, ranging between 0.5 and 0.9 wt%. The Al content varies between 2.7 and 3.8 wt%. Iron, magnesium, and calcium content are, respectively, ~8, ~16, and 19.5 wt% (analyses 1 and 2 in Table T1). The clinopyroxene is associated with microlitic labradorite ( $\text{An}_{62}$ ) (analyses 1–3 in Table T2) retrogressed into albite (analysis 4 in Table T2).

In the coarse-grained diabase with well-preserved doleritic texture, one type of pyroxene is present in the samples located nearer the top of the hole. It displays a zonation from the core to the rim of the porphyroclast (Sample 180-1109D-48R-3, 63–69 cm [analyses 3–9 in Table T1]). According to Morimoto (1988), the pyroxene composition evolved from a magnesio- ( $\text{Wo}_{39-41}\text{En}_{49-50}\text{Fs}_{10}$ ) to a ferro- ( $\text{Wo}_{36}\text{En}_{45}\text{Fs}_{19}$ ) augite composition. The Al concentration decreases from 3.3 to 1.8 wt%; the iron content increases from the core to the rim. The titanium content is very low but increases from 0.5 to 0.9 wt%. In the coarse-grained diabase, the clinopyroxenes are associated with labradorite ( $\text{An}_{70}$ ) (analyses 5 and 6 in Table T2) depleted in calcium toward the rim ( $\text{An}_{55}$ ) (analyses 7 and 8 in Table T2). At the bottom of the hole in the coarse-grained diabase (Sample 180-1109D-51R-1, 58–67 cm), two types of clinopyroxenes are present, corresponding to subhedral porphyroclasts of augite associated with fibrous ferro-augite. The two clinopyroxenes are associated with unzoned phenocrysts of bytownite ( $\text{An}_{85}$ ) up to 1 cm in size (analyses 9 and 10 in Table T2) and labradorite laths.

In the fine-grained diabase (grain size < 2 mm), the clinopyroxene (Table T1) (Sample 180-1109D-51R-4, 6–9 cm) is a ferro-augite ( $\text{Wo}_{36}\text{En}_{42-46}\text{Fs}_{18-21}$ ). The Ti content is  $\sim 0.98 \pm 0.2$  wt%. The Al content varies between 2.03 and 3.62 wt% and does not change significantly with depth and texture (coarse- to fine-grained diabase). The Fe, Mg, and Ca contents are constant, at ~12, 15, and 19 wt% in clinopyroxenes (analyses 10–12 in Table T1). In the fine-grained diabase, the clinopyroxenes are associated with labradorite, with composition ranging between  $\text{An}_{75}$  and  $\text{An}_{55}$  (analyses 11–14 in Table T2).

---

T1. Clinopyroxene analyses, p. 18.

---



---

T2. Plagioclase analyses, p. 20.

---

### Site 1118 Diabase

The clinopyroxenes from the Site 1118 diabase have an augite composition ( $\text{Wo}_{40}\text{En}_{46}\text{Fs}_{14}$ ) (analyses 19–21 in Table T1). The Ti content is low (~0.5 wt%), and the Al content varies between 1.9 and 2.3 wt%. The Fe (7.5 wt%), Mg (16.5 wt%), and Ca (20 wt%) contents are constant. The associated plagioclases are either andesine ( $\text{An}_{45}$ ) or labradorite ( $\text{An}_{60-65}$ ).

In the coarse-grained zones, two distinct clinopyroxenes, either augites ( $\text{Wo}_{37}\text{En}_{45}\text{Fs}_{16}$ ) (analyses 22 and 27 in Table T1) or pigeonites ( $\text{Wo}_{9-13}\text{En}_{46}\text{Fs}_{40-44}$ ) (analyses 23–26 in Table T1), coexist, and the associated plagioclase is a labradorite ( $\text{An}_{55-65}$ ) (analyses 21–23 in Table T2) very often retrogressed into albite ( $\text{An}_5$ ) (analyses 19, 20, and 25 in Table T2).

### Site 1117 Gabbro

At Site 1117, the clinopyroxene has a ferro-augite ( $\text{Wo}_{37-50}\text{En}_{40-30}\text{Fs}_{20-23}$ ) composition (analyses 13–18 in Table T1). Their compositions are characterized by very low aluminum (0.15 wt%) and titanium contents (<1 wt%). A few grains display higher Al contents, up to 2.3 wt%. The Ca content is constant at ~19 wt%, whereas Fe and Mg contents range, respectively, between 13 and 23 wt% and 6 and 15 wt%. The clinopyroxene was associated with a magmatic plagioclase; however, primary magmatic plagioclases were not analyzed because of the high degree of weathering of the rocks. Indeed, the plagioclase is totally transformed into albite (analyses 15–18 in Table T2).

Ilmenites with variable composition were analyzed in the diabbases and the gabbro. The low sum of oxide components is indicative of alteration (Table T3). Oxide grains have very variable compositions from one sample to another wherever they are present (diabase, gabbro, or basaltic rocks). They display Mn contents that range between 5.4 and 0.4 wt%, Ti contents that range between 18 and 32 wt%, and Fe contents that range between 61 and 71 wt%. At Site 1117, the titanomagnetite is rimmed by sphene.

---

T3. Ilmenite analyses, p. 22.

---

## Secondary Mineralogy

The diabbases from Sites 1109 and 1118 and the gabbro from Site 1117 contain various amounts of secondary phases, such as amphiboles and sphene (only observed in the Site 1117 gabbro), chlorite, epidote, zoisite, titanite, and zeolites, observed in all studied mafic rocks. These minerals are representative of low-grade metamorphism. Only the composition of some amphiboles, chlorites, and epidotes will be discussed in the following sections.

### Amphiboles

According to the classification of Leake (1978), the amphiboles developed after clinopyroxene at Site 1117 display a magnesiohornblende to actinolitic hornblende composition (Sample 180-1117A-12R-1, 29–34 cm) with high Cl and F contents, indicating the presence of water-rich fluid during their crystallization (Table T4). Amphibole porphyroclasts are zoned, the Ti content decreases from 1.054 to 0.67 wt%, and the Al and Na contents decrease from 7.25 and 2.5 wt% to 4.6 and 1.4 wt%, respectively. The rim composition of the hornblende porphyro-

---

T4. Amphibole, epidote, and clinzoisite analyses, p. 23.

---

clast is similar to the composition of the fibrous green actinolitic hornblende.

### Chlorites

Chlorite (Table T5) is present in three distinctive structural sites. At Site 1117, chlorite develops in a symplectite texture at the contact between the clinopyroxene and the plagioclase; it consists of a very fine association of albite and brunsvigite. A ripidolitic chlorite present as unoriented patches replacing clinopyroxenes is largely developed in Site 1117 gabbro and in the diabase at Sites 1119 and 1118. Finally, a green oolitic chamoisite associated with glauconite developed in veins from all sites.

### Epidote and Zoisite

Epidote and clinozoisite (Table T4) are present as very small grains in the brecciated rocks from all sites. They also appear filling veins as euhedral grains associated with quartz.

## Conditions of Intrusion and Subsequent Metamorphism of Mafic Rocks

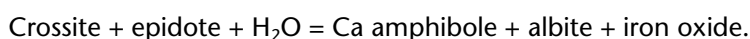
### Conditions of Intrusion

The  $Al^{IV}/Al^M$  diagram (Fig. F3) used to discriminate between pyroxenes from high- and low-pressure origins (Aoki and Shiba, 1973) clearly indicates a shallow level of intrusion for both the diabbases and the gabbro. Indeed, the magmatic clinopyroxenes from all the studied samples plot in the medium-pressure granulite field and low-pressure field of igneous rocks. Clinopyroxenes from the Southwest Indian Ridge oceanic gabbro (Hébert et al., 1991) and from Leg 149, Site 900 gabbro from the Iberian Abyssal Plain (Cornen et al., 1996) are also reported on the diagram and display similar compositions.

### Retrograde Evolution

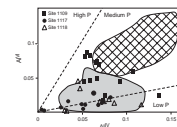
At Site 1117, the petrological observations indicate that the retrograde evolution started with the development of brown to green hornblende amphibole. Concentrically zoned amphibole grains indicate disequilibrium but may provide some record of changing conditions during the growth of the amphiboles. The pale greenish overgrowths on the extreme rims of the brown porphyroclast grains are thought to have formed during the cooling of the rock body. Indeed, experimental data has shown that the Ti content is temperature dependent (Liou et al., 1974; Helz, 1973) and decreases with decreasing temperature. The amphibole compositions presented in Table T4 indicate a decrease in Ti content from the core to the rim of the porphyroclast.

The Al and Na content of amphiboles in metamorphic and magmatic rocks is pressure dependent, decreasing with a fall in pressure (Liou et al., 1974; Moody et al., 1983). Moreover, the buffering reaction that relates the crossite to the Ca amphibole-bearing greenschist facies transition has been determined to be (Brown, 1974)



T5. Chlorite analyses, p. 24.

F3.  $Al^M$  vs.  $Al^{IV}$  diagram for clinopyroxenes, p. 16.





the temperature evolution displays a discrete difference between the footwall (Site 1117) and the hanging wall (Sites 1118 and 1109) margins for the subgreenschist stage, showing higher temperature conditions (~30°–50°C) at Site 1117. These temperatures calculated on the metamorphic rocks give thermal paleogradients that are in good agreement with the present-day thermal gradients obtained at the sites during Leg 180 (see Fig. F2), indicating 95°–100°C/km above the active normal fault itself (Sites 1117 and 1108) and 31°–60°C/km on the hanging wall (Sites 1118 and 1109). This suggests that the different thermal regime between the footwall and the hanging wall, aided by the circulation of hydrothermal fluids, was efficient since the beginning of the rifting.

The texture developed by the metamorphic minerals in the metabasites does not vary a lot in the studied samples. The areal extent of rocks that contain aligned metamorphic minerals is much less than those in which minerals are randomly oriented or radiating. Aligned quartz or chlorite is evident only at Site 1117, which is located on the active normal fault. At this site, the brittle behavior of plagioclase and amphibole and the ductile behavior of quartz grains (Kirby, 1985) recrystallized in the foliation plane suggest that ductile deformation at Site 1117 occurred under greenschist to subgreenschist conditions. The presence of similar mineralogical assemblages in veins developed in all the sites suggests that the ductile deformation at Site 1117 occurred synchronously with the brittle deformation that is very well represented in the Moresby Seamount. It can be concluded that the last stages of the retrograde metamorphism must be attributed to the activity of the active normal fault that emerges at Site 1117.

Moreover, the geochronological data have shown that the Moresby Seamount basement was not thermally reset by subsequent rifting (Monteleone et al., this volume). That the crust remained cool during thinning is confirmed by the petrological data obtained on the diabase and gabbro from Sites 1117, 1118, and 1109, and this is true not only for the last million years but since the initiation of the rifting. This “cold” thermal regime in the upper crust is difficult to explain, considering the extensional setting. A solution is to consider that a major component of crustal thinning results from flow of the lower crust (Taylor and Huchon, this volume) and that the thermal effects of the thinning have yet to be transmitted to the upper crust. This is in agreement with the seismic tomography study, which indicates that the crust thins to an average thickness of 15–20 km flanking Moresby rift. This may help explain the geometry of numerous present-day passive margins where there is a lack of evidence for lower crust at the ocean-continent transition zone (Gardien et al., 2000).

## CONCLUSIONS

Petrological investigations indicate that the diabbases at Sites 1109 and 1118 show a typical intersertal texture between plagioclase and augite and chilled margin expressed by grain size reduction at the contact with a second sill/dyke injection. Gabbro at Site 1117 shows a typical gabbroic texture with the following order of crystallization: plagioclase, pyroxene, and quartz. The secondary mineralogy developed in the gabbro and diabbases are typical of greenschist to subgreenschist facies conditions. This evolution is synchronous with the deformation (brittle to ductile) developed in the rocks at Site 1117 that

is considered to be caused by present-day extension. In agreement with geochronological data, our results show that over the last 8 m.y. the upper crust in the Woodlark Basin was not thermally reset by subsequent heat supply.

## **ACKNOWLEDGMENTS**

This research used samples and/or data provided by the Ocean Drilling Program (ODP). ODP is sponsored by the U.S. National Science Foundation (NSF) and participating countries under management of Joint Oceanographic Institutions (JOI), Inc. Funding for this research was provided by groupe ad-hoc "OCEANS" INSU-CNRS, 1999.

## REFERENCES

- Abers, G.A., 1991. Possible seismogenic shallow-dipping normal faults in the Woodlark-D'Entrecasteaux extensional province, Papua New Guinea. *Geology*, 19:1205–1208.
- Abers, G.A., Mutter, C.Z., and Fang, J., 1997. Shallow dips of normal faults during rapid extension: earthquakes in the Woodlark-D'Entrecasteaux rift system, Papua New Guinea. *J. Geophys. Res.*, 102:15301–15317.
- Abers, G.A., and Roecker, S.W., 1991. Deep structure of an arc-continent collision: earthquake relocation and inversion for upper mantle *P* and *S* wave velocities beneath Papua New Guinea. *J. Geophys. Res.*, 96:6379–6401.
- Aoki, K., and Shiba, I., 1973. Pyroxenes from lherzolite inclusions of Itinome-gata, Japan. *Lithos*, 6:41–51.
- Apted, J.M., and Liou, J.G., 1983. Phase relations among greenschist, epidote-amphibolite, and amphibolite in a basaltic system. *Am. J. Sci.*, 283A:328–354.
- Baldwin, S.L., Lister, G.S., Hill, E.J., Foster, D.A., and McDougall, I., 1993. Thermochronologic constraints on the tectonic evolution of active metamorphic core complexes, D'Entrecasteaux Islands, Papua New Guinea. *Tectonics*, 12:611–628.
- Brown, E.H., 1974. Comparison of the mineralogy and phase relations of blueschists from North Cascades, Washington, and greenschists from Otago, New Zealand. *Bull. Geol. Soc. Am.*, 85:333–344.
- , 1977. The crossite content of Ca-amphiboles as a guide to pressure of metamorphism. *J. Petrol.*, 18:53–72.
- Cathelineau, M., and Nieva, D., 1985. A chlorite solid solution geothermometer: the Loz Azufres (Mexico) geothermal system. *Contrib. Mineral. Petrol.*, 91:235–244.
- Cornen, G., Beslier, M.-O., and Girardeau, J., 1996. Petrology of the mafic rocks cored in the Iberia Abyssal Plain. In Whitmarsh, R.B., Sawyer, D.S., Klaus, A., and Masson, D.G. (Eds.), *Proc. ODP, Sci. Results*, 149: College Station, TX (Ocean Drilling Program), 449–469.
- Davies, H.L., and Jaques, A.L., 1984. Emplacement of ophiolite in Papua New Guinea. In Gass, I.G., Lippar, S.J., and Shelton, A.W. (Eds.), *Ophiolites and Oceanic Lithosphere*. Spec. Publ.—Geol. Soc., London, 13:341–350.
- Gardien, V., Arnaud, N., and Desmurs, L., 2000. Petrology and Ar-Ar dating of granulites from the Galicia Bank: African craton relics in Western Europe. *Geod. Acta*, 13:103–1117.
- Hamilton, W.B., 1979. *Tectonics of the Indonesian Region*. Geol. Surv. Prof. Pap. U.S., 1078.
- Hébert, R., Constantin, M., and Robinson, P.T., 1991. Primary mineralogy of Leg 118 gabbroic rocks and their place in the spectrum of oceanic mafic igneous rocks. In Von Herzen, R.P., Robinson, P.T., et al., *Proc. ODP, Sci. Results*, 118: College Station, TX (Ocean Drilling Program), 3–20.
- Helz, R.T., 1973. Phase relations of basalts in their melting ranges at  $p_{H_2O} = 5$  kb as a function of oxygen fugacity, Part I. Mafic phases. *J. Petrol.*, 14:249–302.
- Holland, T., and Blundy, J., 1994. Non-ideal interactions in calcic amphiboles and their bearing on amphibole-plagioclase thermometry. *Contrib. Mineral. Petrol.*, 116:433–447.
- Jaques, A.L., and Chappell, B.W., 1980. Petrology and trace element geochemistry of the Papuan ultramafic belt. *Contrib. Mineral. Petrol.*, 75:55–70.
- Jenner, G.A., 1981. Geochemistry of high-Mg andesites from Cape Vogel, Papua New Guinea. *Chem. Geol.*, 33:307–332.
- Johnson, R.W., and Jaques, A.L., 1980. Continent-arc collision and reversal of arc polarity: new interpretation from a critical area. *Tectonophysics*, 63:111–124.
- Kirby, S.H., 1985. Rock mechanics observations pertinent to the rheology of the continental lithosphere and the location of strain along shear zones. *Tectonophysics*, 119:1–27.

- Leake, B.E., 1978. Nomenclature of amphiboles. *Am. Mineral.*, 63:1023–1052.
- Liou, J.G., 1971. P-T stabilities of laumontite, wairakite, lawsonite and related minerals in system  $\text{CaAl}_2\text{Si}_2\text{O}_8\text{-SiO}_2\text{-H}_2\text{O}$ . *J. Petrol.*, 12:379–411.
- Liou, J.G., Kuniyoshi, S., and Ito, K., 1974. Experimental studies of the phase relations between greenschist and amphibolite in a basaltic system. *Am. J. Sci.*, 274:613–632.
- Liou, J.G., Maruyama, S., and Cho, M., 1987. Very low-grade metamorphism of volcanic and volcanoclastic rocks-mineral assemblages and mineral facies. In Frey, M. (Ed.), *Very Low-Grade Metamorphism*: New York (Blackie and Son), 59–113.
- Lock, J., Davies, H.L., Tiffin, D.L., Murakami, F., and Kisomoto, K., 1987. The Trobriand subduction system in the western Solomon Sea. *Geo-Mar. Lett.*, 7:129–134.
- Monnier, C., Girardeau, J., Pubellier, M., and Permana, H., 2000. L'Ophiolite de la chaîne centrale d'Irian Jaya (Indonésie): évidences pétrologiques et géochimiques pour une origine dans un bassin d'arrière arc. *C. R. Acad. Sci., Ser. Ila: Sci. Terre Planètes*, 331:691–699.
- Moody, J.B., Meyer, D., and Jenkins, J.E., 1983. Experimental characterization of the greenschist/amphibolite boundary in mafic systems. *Am. J. Sci.*, 283:48–92.
- Morimoto, N., 1988. Nomenclature of pyroxenes. *Am. Mineral.*, 73:1123–1133.
- Nimis, P., and Pulmer, P., 1998. Clinopyroxene geobarometry of magmatic rocks: part 1: an expanded structural geobarometer for anhydrous and hydrous, basic to ultrabasic systems. *Contrib. Mineral. Petrol.*, 133:314–327.
- Otten, M.T., 1984. The origin of brown hornblende in the Artfjället gabbro and dolerites. *Contrib. Mineral. Petrol.*, 86:189–199.
- Plyusnina, L.P., 1982. Geothermometry and geobarometry of plagioclase-hornblende bearing assemblages. *Contrib. Mineral. Petrol.*, 80:140–146.
- Powell, W.G., Carmichael, D.M., and Hodgson, C.J., 1993. Thermobarometry in a subgreenschist to greenschist transition in metabasites of the Abitibi greenstone belt, superior Province. *Can. J. Metamorph. Geol.*, 11:165–178.
- Shipboard Scientific Party, 1999a. Site 1109. In Taylor, B., Huchon, P., Klaus, A., et al., *Proc. ODP Init. Repts.*, 180, 1–298 [CD-ROM]. Available from: Ocean Drilling Program, Texas A&M University, College Station, TX 77845-9547, U.S.A.
- , 1999b. Site 1118. In Taylor, B., Huchon, P., Klaus, A., et al., *Proc. ODP Init. Repts.*, 180, 1–213 [CD-ROM]. Available from: Ocean Drilling Program, Texas A&M University, College Station, TX 77845-9547, U.S.A.
- Spear, F.S., 1981. An experimental study of hornblende stability and compositional variability in amphibolite. *Am. J. Sci.*, 281:697–734.
- Stakes, D., Mével, C., Cannat, N., and Chaput, T., 1991. Metamorphic stratigraphy of Hole 735B. In Von Herzen, R.P., Robinson, P.T., et al., *Proc. ODP, Sci. Results*, 118: College Station, TX (Ocean Drilling Program), 153–180.
- Taylor, B., Goodliffe, A., Martinez, F., and Hey, R., 1995. Continental rifting and initial sea-floor spreading in the Woodlark Basin. *Nature*, 374:534–537.
- Wernicke, B., 1995. Low-angle normal faults and seismicity: a review. *J. Geophys. Res.*, 100:20159–20174.
- Winkler, H.G.F., 1979. *Petrogenesis of Metamorphic Rocks* (5th ed.): New York (Springer-Verlag).

Figure F1. Regional setting and tectonics of the Papua New Guinea–Solomon Islands region. MT = Moresby transform fault, ST = Simbo transform fault, DE = D’Entrecasteaux Islands, MS = Moresby Seamount, G = Goodenough Island, F = Fergusson Island, N = Normanby Island. The top inset shows the geographic location of the study area (modified from Shipboard Scientific Party, 1999b).

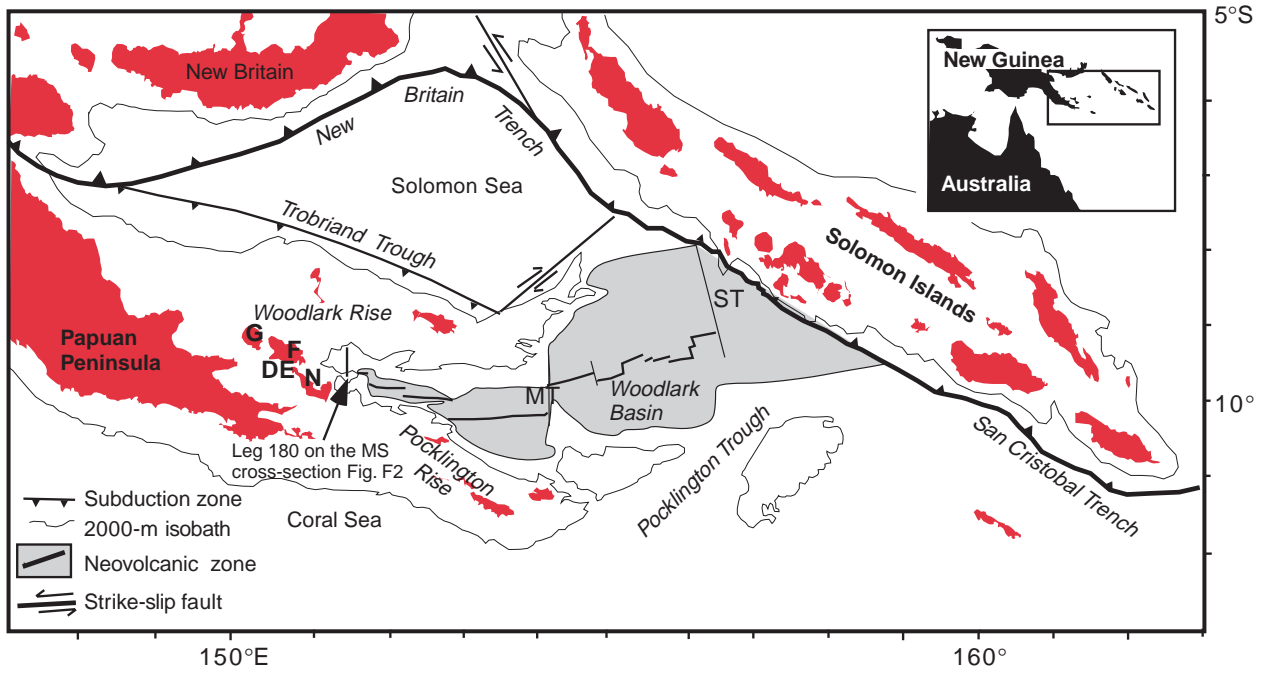
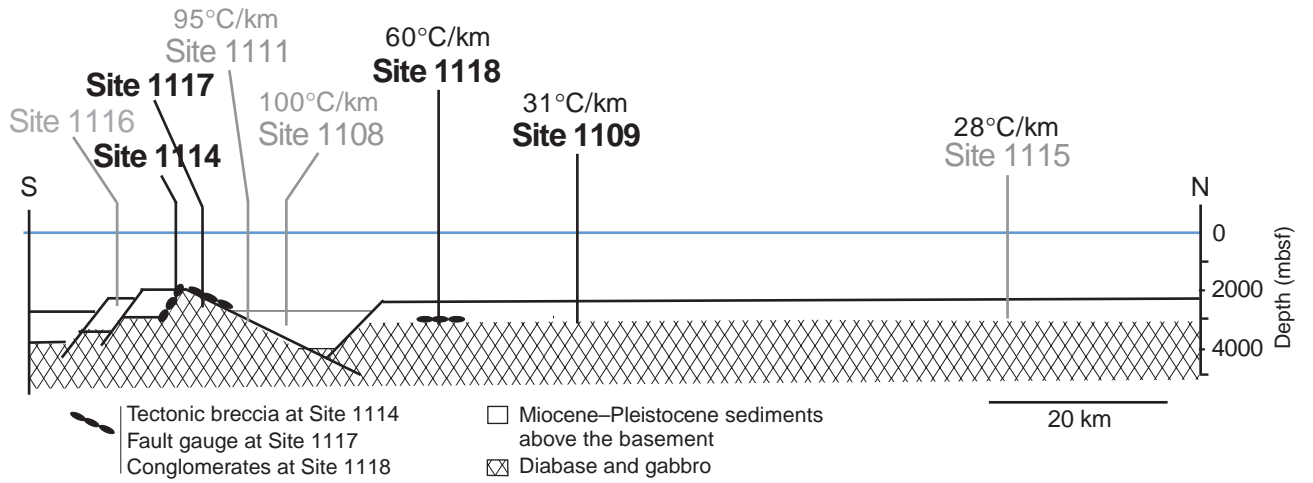
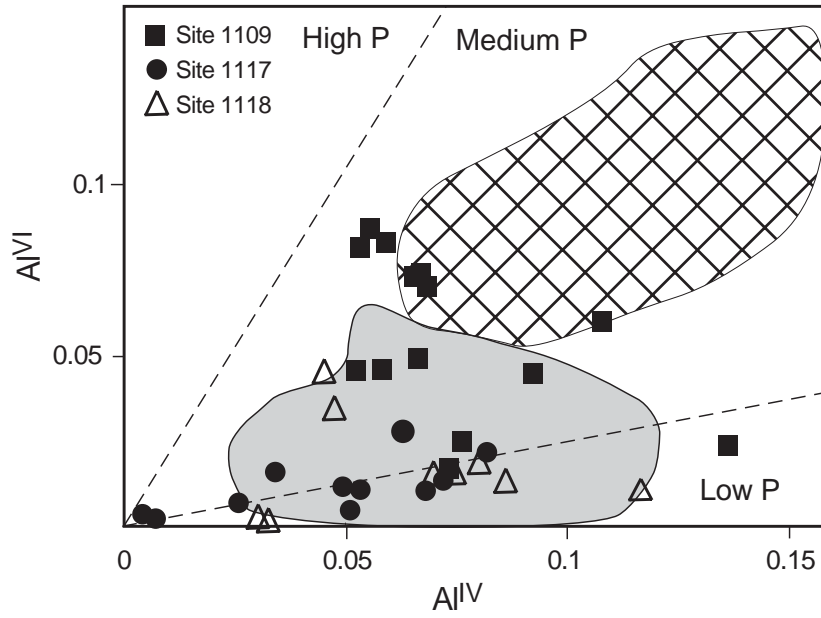


Figure F2. Schematic cross-section of Leg 180 sites. Basement sites are highlighted in bold. Estimates of the thermal gradients obtained at five sites during Leg 180 are shown (after Shipboard Scientific Party, 1999b).



**Figure F3.**  $Al^M$  vs.  $Al^V$  diagram for clinopyroxenes (the structural formula was calculated on the basis of six oxygens and four cations) of dolerites (Sites 1109 and 1118) and gabbros (Site 1117) from the Woodlark Basin. Clinopyroxenes from diabase (Sites 1109 and 1118) plot in the medium- to low-pressure field, whereas clinopyroxenes from gabbro (Site 1117) plot only in the low-pressure fields. The shaded area is gabbros and ferrogabbros from the Iberia Abyssal Plain and the Gorringe Bank of the Galicia margin in Portugal (data from Cornen et al. 1996). The cross-hatched area is clinopyroxenes from the Southwest Indian Ridge (data from Hébert et al., 1991; Stakes et al., 1991). Pressure (P) domains are from Aoki and Shiba (1973).



**Figure F4.** Pressure-temperature path for the gabbro and diabase from Sites 1118, 1109, and 1117. The evolution shows the magmatic crystallization (dated at  $66.4 \pm 1.5$  Ma) followed by cooling and retrograde greenschist alteration (dated at  $31 \pm 0.9$  Ma) and, finally, the subgreenschist deformation and metamorphism (undated) related to rifting. Pressure conditions during intrusion were determined with the Nimis and Pulmer (1998) barometer. Reactions used in the diagram are from Powell et al., (1993): (1)  $Zo + Grt + Qtz + H_2O = Phr$ ; (2)  $Czo + Act + H_2O = Pump + Chl + Qtz$ ; (3)  $Act + Pump + Ep + H_2O = Phr + Chl$ ; (4)  $Phr + Ep + Chl + H_2O = Pump + Qtz$ ; and (5)  $Act + Pump + Ep + Qtz = Phr + Chl$ . Epi-out and Sph-out are after Apte and Liou (1983); Cpx-in is after Spear (1981) for QFM (quartz-fayalite-magnetite) buffer; Chl-out is after Liou (1971), after Winkler (1979). The  $Al_{tot}$ -Hbl barometer is after Plyusnina (1982). Dashed lines = temperatures obtained using the hornblende-plagioclase thermometer of Holland and Blundy (1994), solid lines = temperatures obtained with the Otten (1984) hornblende thermometer. I, II, and III = temperature conditions obtained using the Cathelineau and Nieva (1985) thermometer on the third generation of chlorites. Chl = chlorite, ab = albite, act = actinite, qtz = quartz, pl = plagioclase, Cc = calcite, hbl = hornblende, zo = zoisite, V = vapor, ep = epidote, sph = sphalerite, cpx = clinopyroxene. Grt = garnet, Czo = clinozoisite, Phr = prehnite, Act = actinolite, Pump = pumpellinite, Ep = epidote, Chl = chlorite.

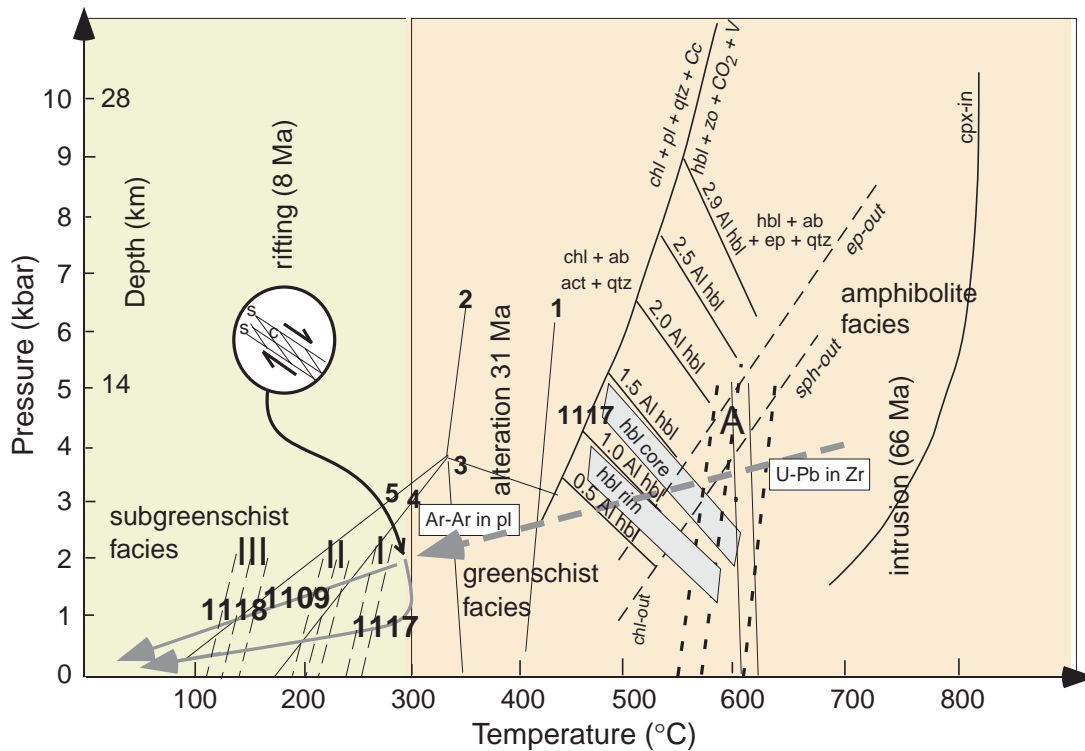


**Table T1.** Selected analyses of clinopyroxenes, Sites 1109, 1118, and 1117. (Continued on next page.)

Core, section, interval (cm):	180-1109D-41R-3, 72-74				180-1109D-48R-3, 63-69					180-1109D-51R-4, 6-9			180-1117A-11R-1, 40-44		
	Basalt		Coarse-grained diabase							Fine-grained diabase			Gabbro		
Matrix:	1	2	3	4	5	6	7	8	9	10	11	12	13	14	15
Analysis number:	1	2	3	4	5	6	7	8	9	10	11	12	13	14	15
Major element oxide (wt%):															
SiO <sub>2</sub>	52.66	50.77	51.54	52.98	52.34	53.43	52.79	53.53	53.62	49.91	51.12	51.22	50.92	50.62	49.80
TiO <sub>2</sub>	0.49	0.94	0.72	0.66	0.63	0.73	0.66	0.72	0.65	0.98	0.88	0.78	0.56	0.85	0.00
Cr <sub>2</sub> O <sub>3</sub>	0	0	0.12	0.54	0.61	0.32	0.63	0.63	0.72	0	0	0.34	0.00	0.00	0.00
Al <sub>2</sub> O <sub>3</sub>	2.65	3.82	3.13	3.27	3.25	3.23	3.2	3.15	3.31	3.62	2.11	2.03	2.01	2.30	0.15
FeO <sub>(tot)</sub>	6.44	7.45	6.35	5.97	6	6.36	6.06	6.1	6.48	11.24	12.34	13.02	16.13	12.53	23.06
Fe <sub>2</sub> O <sub>(C)</sub>	1.22	0.09	0	0	0	0	0	0	0	2.7	0.83	1.03	0.65	1.01	0.49
FeO(C)	5.34	7.37	6.35	5.97	6	6.36	6.06	6.48	6.48	8.81	11.6	12.09	15.54	11.63	22.62
MnO	0.2	0.17	0.19	5.97	0.13	0.15	0.16	0.16	0.15	0.28	0.28	0.34	0.38	0.32	0.60
MgO	17.26	15.92	16.52	16.03	16.15	16.81	16.63	16.7	17.03	16.21	14.74	14.85	12.47	14.42	6.90
NiO	0	0	0.04	0	0	0.04	0.04	0.08	0	0	0	0	0.00	0.00	0.00
CaO	19.67	19.52	19.57	20.33	20.13	20.12	19.74	19.67	18.85	17.62	18.04	17.5	17.53	17.94	18.43
Na <sub>2</sub> O	0.24	0.27	0.25	0.29	0.21	0.25	0.21	0.21	0.28	0	0.28	0.27	0.29	0.28	0.18
Total	99.61	98.97	99.21	100.27	99.45	101.44	100.13	100.96	101.09	100.13	99.79	99.99	100.29	99.25	99.11
Si	1.934	1.892	1.9085	1.9415	1.933	1.9321	1.9348	1.9471	1.9455	1.864	1.924	1.927	1.937	1.918	1.994
Ti	0.014	0.026	0.0199	0.0182	0.0175	0.0199	0.0182	0.0196	0.0178	0.028	0.025	0.022	0.016	0.024	0
Cr	0	0	0.0035	0.0157	0.0178	0.009	0.0184	0.0182	0.0207	0	0	0	0	0	0
Al <sup>(IV)</sup>	0.0844	0.1067	0.0799	0.0666	0.0738	0.0725	0.0727	0.0706	0.055	0.136	0.076	0.073	0.063	0.082	0.006
Al <sup>(VI)</sup>	0.049	0.06	0.045	0.083	0.074	0.07	0.073	0.082	0.087	0.024	0.025	0.016	0.028	0.021	0.001
Fe <sup>3+</sup>	0.034	0.0025	0	0	0	0	0	0	0	0.0755	0.0232	0.0292	0.0186	0.0286	0.0148
Fe <sup>2+</sup>	0.1661	0.299	0.1978	0.1822	0.1846	0.1919	0.185	0.1953	0.1975	0.2739	0.3647	0.3786	0.4939	0.3639	0.7567
Mn	0.006	0.005	0.006	0.0059	0.0042	0.0045	0.0051	0.0048	0.0047	0.009	0.009	0.011	0.012	0.01	0.02
Mg	0.945	0.885	0.9115	0.8753	0.8889	0.906	0.9084	0.9055	0.9212	0.903	0.827	0.833	0.708	0.815	0.412
Ni	0	0	0.0012	0	0	0.0011	0.0011	0.0024	0	0	0	0	0	0	0
Ca	0.774	0.779	0.7761	0.7981	0.7966	0.7794	0.7752	0.7666	0.7327	0.705	0.728	0.705	0.715	0.728	0.791
Na	0.017	0.02	0.0183	0.0209	0.0153	0.0176	0.0146	0.015	0.0193	0.019	0.02	0.02	0.021	0.02	0.014
%Wo	40.3	41	38.8	41.7	41	39.9	37.7	40.15	34.8	35.8	37.3	36	36.7	37.3	39.6
%En	49.1	46.5	50.3	48.2	48.7	49.5	49.8	49.6	46.1	45.9	42.4	42.5	36.3	41.8	40.6
%Fs	10.6	12.5	10.8	10	10.2	10.5	10.2	10.2	18.3	18.3	20.3	21.5	27	20.9	20.7

Note: Wo = wollastonite, En = enstatite, Fs = ferrosillite.

Table T1 (continued).

Core, section, interval (cm):	180-1117A-12R-1, 29–34			180-1117A-70R-1, 112–28			180-1118A-74R-2, 133–138			180-1118A-76R-1, 28–38		
Matrix:	Gabbro			Diabase			Coarse-grained diabase			Coarse-grained diabase		
Analysis number:	16	17	18	19	20	21	22	23	24	25	26	27
Major element oxide (wt%):												
SiO <sub>2</sub>	51.33	50.954	52.31	51.897	51.58	52.41	51.22	51.13	50.9	53.14	53.73	53.13
TiO <sub>2</sub>	0.58	0.535	0.113	0.46	0.52	0.45	0.78	0.45	0.4	0.41	0.65	0.52
Cr <sub>2</sub> O <sub>3</sub>	0.00	0.00	0.00	0.00	0.21	0.2	0.00	0	0	0.01	0.01	0.05
Al <sub>2</sub> O <sub>3</sub>	1.886	1.803	0.159	2.284	2.26	1.94	2.03	0.74	0.71	0.66	1.6	2.08
FeO <sub>(tot)</sub>	13.163	14.142	13.341	7.54	8.49	7.77	13.02	26.47	26.86	23.23	19.56	7.68
Fe <sub>2</sub> O(C)	1.35	1.77	0	1.81	2.34	1.59	1.03	0.28	0.86	0	0	0
FeO(C)	11.94	12.55	13.34	5.91	6.38	6.34	12.09	26.22	26.09	23.23	19.56	7.68
MnO	0.383	0.3	0.798	0.18	0.21	0.19	0.34	0.68	0.65	0.55	0.52	0.19
MgO	14.7	14.458	9.64	16.71	16.61	17.1	14.85	15.18	15.88	18.89	17.57	16.43
NiO	0.00	0.00	0.00	0.00	0.00	0.00	0	0	0	0	0.04	0.06
CaO	18.035	17.333	24.286	20.34	19.76	19.98	17.5	5.72	4.69	4.17	6.61	19.64
Na <sub>2</sub> O	0.217	0.245	0.055	0.23	0.27	0.2	0.27	0.11	0.07	0.07	0.09	0.26
Total	100.29	99.77	100.7	99.9	99.98	100.25	99.99	100.18	100.19	101.12	100.38	100.11
Si	1.929	1.931	1.995	1.92	1.914	1.93	1.927	1.969	1.964	1.9889	2.02	1.955
Ti	0.016	0.015	0.016	0.013	0.014	0.013	0.0221	0.013	0.012	0.0116	0.0183	0.016
Cr	0	0	0	0.007	0.006	0.006	0	0	0	0.0002	0.0004	0.0014
Al <sup>(IV)</sup>	0.071	0.069	0.005	0.08	0.086	0.07	0.073	0.031	0.032	0.047	0	0.045
Al <sup>(VI)</sup>	0.013	0.011	0.002	0.019	0.013	0.014	0.016	0.002	0.002	0.035	0.071	0.045
Fe <sup>3+</sup>	0.0382	0.0502	0	0.0502	0.0651	0.939	0.0439	0.0292	0.0082	0.0248	0	0
Fe <sup>2+</sup>	0.3749	0.3963	0.4254	0.1826	0.1972	0.1947	0.3796	0.8438	0.8406	0.7256	0.6081	0.2364
Mn	0.012	0.01	0.026	0.006	0.007	0.006	0.011	0.022	0.021	0.0175	0	0
Mg	0.824	0.817	0.548	0.921	0.919	0.939	0.833	0.871	0.913	0	0.0166	0.006
Ni	0	0	0	0	0	0	0	0	0	0	0.0011	0.0018
Ca	0.726	0.704	0.992	0.806	0.786	0.788	0.705	0.1236	0.194	0.1671	0.2662	0.7742
Na	0.016	0.018	0.004	0.017	0.019	0.015	0.02	0.008	0.005	0.0048	0.0063	0.0185
%Wo	36.8	35.6	49.8	41	39.8	40	36	12	10	10	13	37.2
%En	41.7	41.3	37.5	46.9	46.5	47.6	42.5	44	46	53	50	45.1
%Fs	21.6	23.1	22.7	12.2	13.7	12.4	21.5	44	44.5	37	37	11.8

**Table T2.** Selected analyses of plagioclases, Sites 1109, 1118, and 1117. (Continued on next page.)

Core, section, interval (cm):	180-1109D-41R-3, 72-74		180-1109D-48R-3, 63-79			180-1109D-51R-4, 6-9				180-1109D-51R-4, 58-67			180-1117A-11R-1, 40-44			
Matrix:	Basalt		Coarse-grained diabase			Fine-grained diabase							Gabbro			
Analysis number:	1	2	3	4	5	6	7	8	9	10	11	12	12	13	14	15
Major element oxide (wt%):																
SiO <sub>2</sub>	68.88	52.99	51.29	55.72	54.04	49.79	51.94	53.84	54.94	46.921	47.118	51.81	71.32	67.69	67.92	68.47
Al <sub>2</sub> O <sub>3</sub>	20.289	27.536	28.33	28.27	28.58	30.4	29.26	28.34	27.55	33.057	32.97	29.95	17.20	20.91	20.41	20.17
MgO	0.00	0.622	0.25	0.1	0.12	0.22	0.13	0.07	0.1	0.164	0.202	0.17	0.539	0.00	0.00	0.00
FeO	0.148	1.418	0.55	0.87	0.78	0.615	0.991	1.155	0.79	0.458	0.507	0.84	1.67	0.31	0.09	0.02
CaO	0.164	12.712	13.56	11.23	11.14	15.22	13.26	11.79	10.79	17.34	17.369	13.49	0.35	0.65	0.48	0.32
Na <sub>2</sub> O	11.582	4.487	3.28	4.89	5.01	2.93	4.13	4.76	5.34	1.611	1.762	3.85	8.78	10.99	11.46	11.54
K <sub>2</sub> O	0.054	0.1	0.03	0.08	0.08	0.26	0.07	0.07	0.05	0.164	0.202	0.08	0.03	0.037	0.106	0.059
Total	101.2	99.94	99.93	100.02	99.56	100.19	99.46	99.53	99.74	101.30	99.85	100.19	99.90	100.59	100.52	100.58
Ab	98.9	38.8	30.39	43.86	46.97	25.51	35.92	42.04	47.08	14.25	15.33	33.9	97.6	96.62	97.18	98.16
An	0.8	60.7	69.43	55.45	52.54	73.25	63.7	57.55	52.61	84.79	83.51	65.7	2.18	3.16	2.23	1.51
Or	0.3	0.6	0.18	0.25	0.49	1.24	0.38	0.41	0.31	0.95	1.16	4.5	0.22	0.21	0.59	0.33

Note: Ab = albite, An = anorthite, Or = orthoclase.

Table T2 (continued).

Core, section, interval (cm):	180-1118A-74R-2, 133–138			180-1118A-76R-1, 28–38 cm			
Matrix:	Coarse-grained diabase			Coarse-grained diabase			
Analysis number:	16	17	18	19	20	21	22
Major element oxide (wt%):							
SiO <sub>2</sub>	63.73	67.54	53.48	56.83	54.63	57.59	68.04
Al <sub>2</sub> O <sub>3</sub>	21.23	20.3	29.24	28.17	27.6	26.86	21.01
MgO	0.01	0.03	0.12	0.07	0.12	0.06	0
FeO	0.7	0.12	1.18	0.74	0.97	0.68	0.15
CaO	1.37	0.83	12.4	10.55	11.33	9.1	0.87
Na <sub>2</sub> O	10.78	10.7	4.51	3.34	5.32	6.56	10.81
K <sub>2</sub> O	0.01	0.03	0.08	0.11	0.09	0.09	0
Total	101.84	99.54	101.05	99.85	100.09	100.99	100.92
Ab	93.36	95.75	39.53	36.16	45.69	56.29	95.75
An	6.56	4.09	60.02	63.03	53.79	43.18	4.24
Or	0.07	0.016	0.045	0.8	0.53	0.53	0

**Table T3.** Selected analyses of ilmenite, Sites 1117, 1118, and 1109.

Core, section, interval (cm):	180-1117A-11R-1, 40-44		180-1118A-74R-2, 133-138		180-1118A-76R-1, 28-38		180-1109D-51R-1, 58-67			180-1109D-51R-4, 6-9		
Matrix:	Gabbro		Coarse-grained diabase		Coarse-grained diabase		Fine-grained diabase			Fine-grained diabase		
Mineral:	Ilmenite	Ilmenite	Ilmenite	Ilmenite	Ilmenite	Ilmenite	Ilmenite	Ilmenite	Ilmenite	Ilmenite	Ilmenite	
Major element oxide (wt%):												
SiO <sub>2</sub>	0.12	0.11	0.85	0.19	0.56	1.31	0.11	2.7	0.34	0.08	0.09	
Al <sub>2</sub> O <sub>3</sub>	2	2	1	2	3	3	1	2	2	1	1	
MgO	0.05	0.07	0.10	0.00	0.08	0.17	0.40	0.04	0.66	0.00	0.42	
FeO	61.58	68.74	71.61	68.62	66.19	66.55	71.30	62.72	65.58	61.36	74.25	
MnO	1.64	0.02	2.77	2.49	3.08	1.31	0.43	5.40	3.95	0.61	0.32	
TiO <sub>2</sub>	31.87	27.44	18.50	22.52	21.09	21.12	23.56	21.34	21.93	32.68	18.73	
CaO	0.03	2.63	0.61	0.34	0.42	0.29	0.01	2.42	0.04	0.26	0.01	
Na <sub>2</sub> O	0	0.082	0.12	0.04	0.08	0.03	0	0.04	0	0	0	
K <sub>2</sub> O	0	0.014	0	0	0	0.02	0	0.014	0	0	0.02	
Total	95.12	96.21	93.61	94	90.87	89.32	95.30	91.94	91.50	94.91	93.33	
Al	0.118	0.116	0.09	0.11	0.18	0.21	0.06	0.16	0.14	0.04	0.07	
Ti	1.36	0.81	0.8	0.97	0.93	0.93	1	0.95	0.95	1.43	0.81	
Fe <sup>3+</sup>	0.152	1.258	1.303	0.946	0.966	0.923	1.005	0.932	0.960	0.104	1.311	
Fe <sup>2+</sup>	2.78	2.3	2.16	2.35	2.27	2.35	2.45	2.18	2.2	2.87	2.26	
Mn	0.15	1.26	1.3	0.95	0.97	0.92	0.93	0.93	0.96	0.1	1.31	
Mg	0.08	0	0.14	0.12	0.15	0.07	0.02	0.27	0.19	0.03	0.02	
Ca	0.004	0.007	0.009	0	0.007	0.015	0.033	0.003	0.057	0	0.036	

Table T4. Selected analyses, Site 1117.

Core, section, interval (cm):	180-1117A-11R-1, 46-53			180-1117A-12R-1, 29-34			
	Gabbro			Gabbro			
	Mineral	Act-Hbl	Hbl	Act-Hbl	Epi	Epi	Zoi
Major element oxide (wt%):							
SiO <sub>2</sub>	47.75	45.34	48.13	37.85	37.31	49.6	41.3
Al <sub>2</sub> O <sub>3</sub>	4.23	7.25	4.69	21.51	20.87	20.09	30.39
MgO	10.62	12.75	10.78	0	0	0.44	0.1
Fe <sub>2</sub> O <sub>3</sub>	3.7	7.57	6.69	15.05	15.2	2.66	0.46
FeO	17.34	10.93	16.27	0	0	0	0
MnO	0.23	0.29	0.37	0.04	0.13	0.16	0.04
TiO <sub>2</sub>	0.95	1.05	0.67	0.16	0.08	0.01	0
CaO	10.51	9.2	8.99	23.18	22.82	23.04	21.55
Na <sub>2</sub> O	1.45	2.36	1.33	0	0	0.04	2.88
K <sub>2</sub> O	0.48	0.03	0.25	0	0.02	0.01	0
F	0.4	0.4	0.03	—	—	—	—
Cl	0.26	0.32	0.37	—	—	—	—
Total	97.92	97.5	98.57	97.79	96.43	96.05	96.72
Si	7.13	6.59	6.97	3.25	3.25	3.97	3.53
Al <sup>IV</sup>	0.73	1.14	0.78	0	0	0	0
Al <sup>VI</sup>	0.032	0.155	0.05	2.18	2.15	1.9	3.06
Ti	0.11	0.12	0.07	0.01	0.005	0	0
Fe <sup>2+</sup>	1.797	1.658	1.46	0	0	0	0
Fe <sup>3+</sup>	0.831	0.592	1.32	1.09	1.11	0.178	0.04
Mn	0.03	0.03	0.05	0.003	0.01	0.011	0.003
Mg	2.36	2.76	2.33	0	0	0.053	0.013
Ca	1.72	1.49	1.61	2.13	2.13	1.98	2.058
Na	0.43	0.694	0.393	0	0	0.01	0.478
K	0.093	0.01	0.05	0	0.002	0	0

Notes: Act-Hbl = actinolitic hornblende, Hbl = hornblende, Epi = epidote, Zoi = zoisite.  
— = not analyzed.

**Table T5.** Selected analyses of chlorites from Sites 1117, 1118, and 1109. (Continued on next page.)

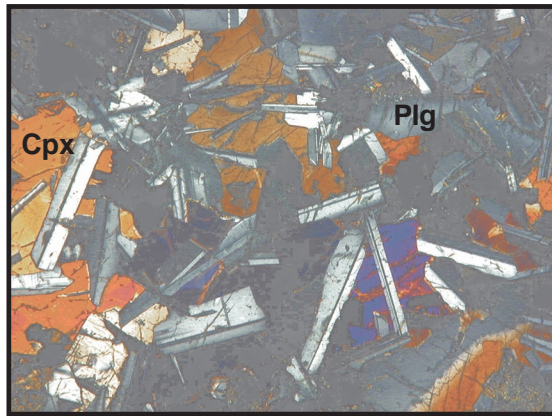
Core, section, interval (cm):	180-1109D-44R-1, 75–88	180-1109D-48R-2, 87–105	180-1109D-51R-4, 6–9	180-1118A-74R-2, 123–138	180-1118A-76R-1, 28–29							
Depth (mbsf):	–750	–782	–797	–898	–910							
Matrix:	Diabase	Diabase	Basalt	Diabase	Fine grained diabase							
Placement:	In vein	After cpx	After cpx	After cpx	After cpx	After cpx	In vein	In vein				
Major element oxide (wt%):												
SiO <sub>2</sub>	28.91	29.3	30.31	30.48	27.92	27.99	28.36	30.48	29.31	28.75	28.91	30.35
Al <sub>2</sub> O <sub>3</sub>	12.08	15.24	15.34	14.86	16.12	16.1	15.07	14.86	13.45	14.82	12.08	15.08
TiO	0.07	0.05	0.04	0	0.07	0.13	0.15	0	0	0.05	0.07	0
FeO	25.16	30.78	27.21	26.53	32.51	31.7	31.87	26.53	32.13	32.52	25.16	32.17
MgO	10.72	11.27	13.69	13.65	8.75	9.13	10.22	13.65	11.25	10.39	10.72	11.11
CaO	1.05	1.64	1.72	1.27	1.48	1.76	1.06	1.27	1.13	1.24	1.05	1.11
MnO	0.14	0.19	0.17	0.08	0.31	0.39	0.04	0.08	0.22	0.22	0.14	0.23
Cr <sub>2</sub> O <sub>3</sub>	0	0	0	0	0	0	0	0	0	0	0	0
Na <sub>2</sub> O	0.09	0.03	0.12	0.04	0.04	0.06	0.02	0.04	0.05	0.07	0.09	0.03
Total	78.22	88.5	88.6	86.91	87.2	87.26	86.8	86.92	87.54	88.06	78.22	90.09
Si	6.881	6.305	6.378	6.503	6.177	6.169	6.269	6.503	6.437	6.287	6.882	6.426
Al <sup>IV</sup>	<b>1.119</b>	<b>1.695</b>	<b>1.622</b>	<b>1.497</b>	<b>1.823</b>	<b>1.831</b>	<b>1.731</b>	<b>1.497</b>	<b>1.563</b>	<b>1.713</b>	<b>1.118</b>	<b>1.574</b>
Al <sup>VI</sup>	2.27	2.171	2.182	2.24	2.38	2.352	2.196	2.24	1.919	2.107	2.271	2.19
Ti	0.013	0.008	0.006	0	0.012	0.022	0.025	0	0	0.008	0.012	0
Fe	5.008	5.54	4.788	4.734	6.015	5.843	5.891	4.733	5.902	5.947	5.008	5.695
Mg	3.805	3.615	4.294	4.341	2.886	3	3.368	4.342	3.683	3.387	3.802	3.507
Ca	0.268	0.378	0.388	0.29	0.351	0.416	0.251	0.29	0.266	0.291	0.269	0.252
Mn	0.028	0.035	0.03	0.014	0.058	0.073	0.008	0.015	0.041	0.041	0.028	0.042
Cr	0	0	0	0	0	0	0	0	0	0	0	0
Na	0.042	0.013	0.049	0.017	0.017	0.026	0.009	0.018	0.021	0.03	0.041	0.013
Total	19.432	19.76	19.74	19.637	19.718	19.731	19.748	19.638	19.832	19.81	19.432	19.698
T (°C) (Al <sup>IV</sup> ):	118	211	199	179	232	233	214	180	190	214	192	114

Notes: cpx = clinopyroxene. Temperatures calculated using the Cathelineau and Nieva (1985) thermometer are indicated at the bottom of the columns. Bold entries are the value used for the chlorite thermometry.

Table T5 (continued).

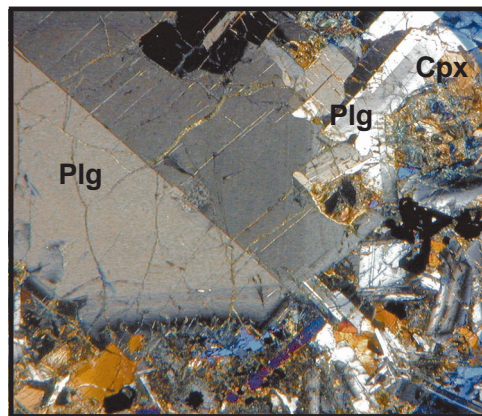
Core, section, interval (cm):	180-1118A-76R-3, 63–69						180-1117A-11R-1, 40–42				180-1117A-12R-1, 29–34		
Depth (mbsf):	–930						–86				–95		
Matrix:	Fine-grained diabase						Undeformed gabbro				Sheared gabbro		
Placement:	In vein		After cpx				In symplectite				After cpx		
Major element oxide (wt%):													
SiO <sub>2</sub>	31.49	30.64	30.62	30.56	31.28	30.52	28.75	28.74	27.48	27.85	29.94	29.65	29.44
Al <sub>2</sub> O <sub>3</sub>	13.57	14	14.68	14.2	15.35	14.09	16.32	17.1	16.07	15.39	14.85	13.76	13.55
TiO	0	0	0.02	0.03	0.01	0	0.01	0.05	0	0	0.09	0	0.03
FeO	30.7	29.78	28.2	31.35	29.07	31.37	33.19	28.12	33.31	33.04	28.8	31.52	33.83
MgO	9.24	11.01	11.89	10.05	10.27	10.33	10.73	8.19	10.21	11.07	14.31	13.87	10.39
CaO	1.26	1.21	1.03	1.02	1.39	1.02	0.16	4.9	0.18	0.3	0.19	0.11	1.1
MnO	0.2	0.23	0.11	0.32	0.14	0.27	0.27	0.25	0.34	0.24	0.21	0.28	0.28
Cr <sub>2</sub> O <sub>3</sub>	0	0	0.01	0	0	0	0	0	0	0	0	0	0
Na <sub>2</sub> O	0.07	0.05	0.04	0.07	0.08	0.08	0.07	0.09	0.13	0.02	0	0.02	0.01
Total	86.53	86.92	86.6	87.6	87.59	87.68	88.59	87.44	87.72	87.91	88.38	89.21	88.62
Si	6.888	6.656	6.606	6.638	6.685	6.625	6.055	6.235	6.056	6.112	6.348	6.335	6.436
Al <sup>IV</sup>	1.112	1.344	1.394	1.362	1.315	1.375	1.945	1.765	1.944	1.888	1.652	1.665	1.564
Al <sup>VI</sup>	2.387	2.241	2.339	2.274	2.551	2.23	2.238	2.607	2.23	2.092	2.059	1.8	1.927
Ti	0	0	0.03	0.005	0.002	0	0.001	0.008	0	0	0.014	0	0.005
Fe	5.616	5.41	5.088	5.695	5.196	5.695	6.035	5.102	6.319	6.065	5.107	5.632	6.185
Mg	3.013	3.565	3.824	3.254	3.272	3.343	3.475	2.65	3.354	3.622	4.524	4.419	3.385
Ca	0.295	0.282	0.238	0.237	0.318	0.237	0.038	1.139	0.043	0.07	0.043	0.025	0.258
Mn	0.037	0.042	0.02	0.059	0.025	0.05	0.049	0.045	0.063	0.045	0.037	0.05	0.051
Cr	0	0	0.002	0	0	0	0	0	0	0	0	0	0
Na	0.03	0.021	0.017	0.029	0.033	0.034	0.029	0.036	0.055	0.007	0	0.01	0.004
Total	19.378	19.562	19.532	19.554	19.397	19.589	19.867	19.588	19.884	19.901	19.783	19.937	19.815
T (°C) (Al <sub>IV</sub> ):	117	155	166	157	150	160	251	222	250	242	204	206	190

**Plate P1.** Photomicrographs of diabase. 1. Preserved magmatic texture in coarse-grained diabase (Sample 180-1109D-48R-3, 63–69 cm) (cross-polarized transmitted light). 2. Porphyroclastic plagioclase in diabase (Sample 180-1109D-51R-3, 58–67 cm) (cross-polarized transmitted light). 3. Basaltic texture of the chilled margin in diabase (Sample 180-1109D-41R-3, 63–69 cm) (cross-polarized transmitted light). 4. Preserved magmatic texture in fine-grained diabase (Sample 180-1109D-51R-4, 6–9 cm) (plane-polarized transmitted light). 5. Poorly preserved magmatic texture in Site 1114 brecciated diabase (Sample 180-1114A-35R-1, 24–27 cm) (plane-polarized transmitted light). 6. Retrogressed and deformed diabase at Site 1114 (plane-polarized transmitted light). Cpx = clinopyroxene, Plg = plagioclase, Glau = glaucony, Chl = chlorite, Calc = calcite, oxi = iron oxide.



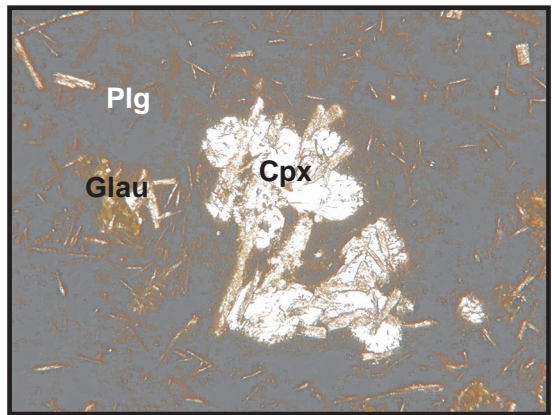
1

2 mm



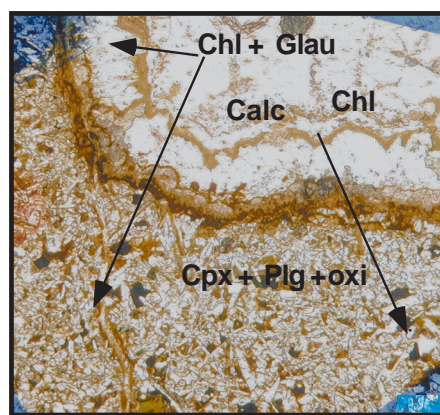
2

2 mm



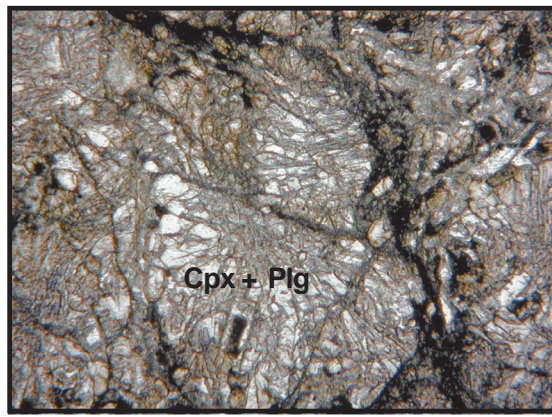
3

1 mm



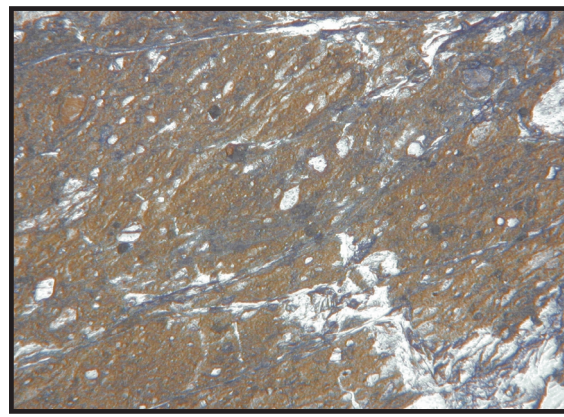
4

2 mm



5

2 mm



6

1 mm

**Plate P2.** Photomicrographs of diabase from Site 1118. **1.** Undeformed fine-grained diabase. Note the presence of chlorite patches replacing clinopyroxene (plane-polarized transmitted light). **2.** Undeformed pegmatitic diabase. Note the abrupt reduction of spectacular dendritic iron oxide (plane-polarized transmitted light). **3.** Contact between a coarse-grained diabase and a fine-grained diabase. Note the abrupt reduction in grain size across the contact (plane-polarized transmitted light). **4.** Grain size reduction in the brecciated diabase (cross-polarized transmitted light). Cpx = clinopyroxene, Plg = plagioclase, Ilm = ilmenite, Chl = chlorite.

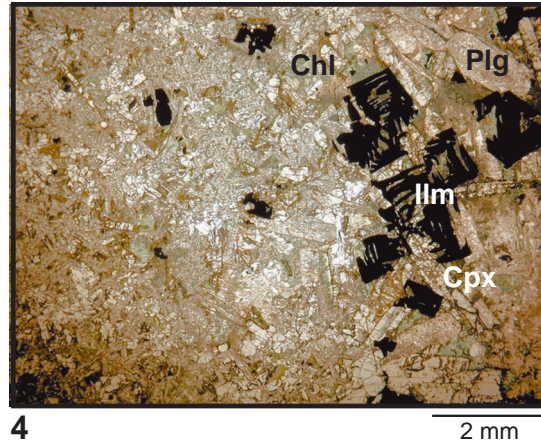
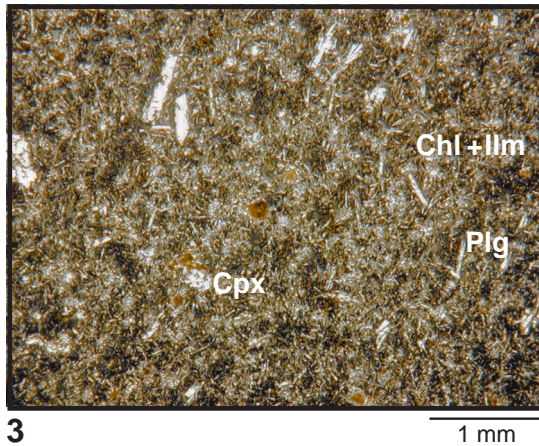
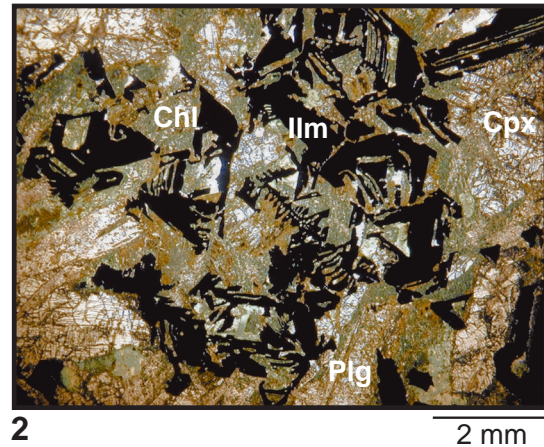
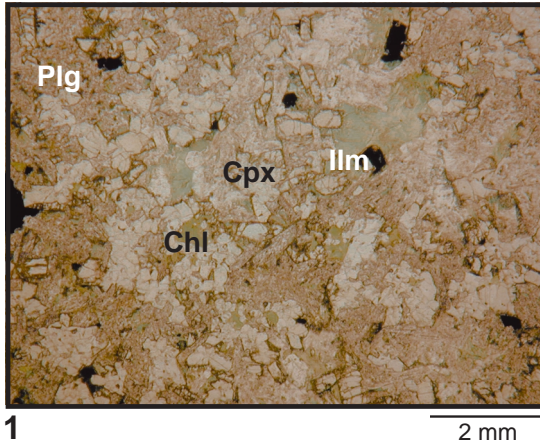
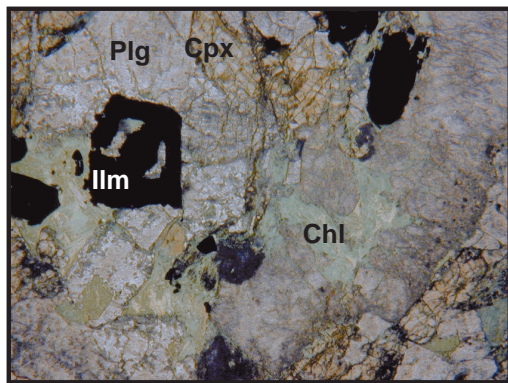
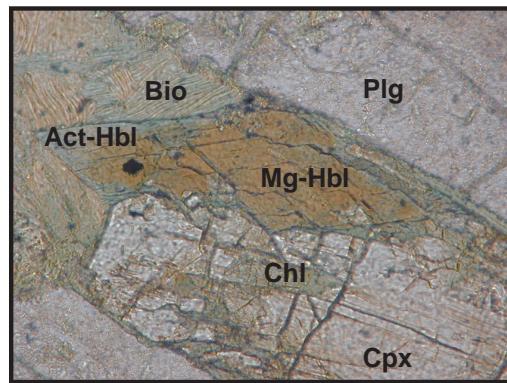


**Plate P3.** Photomicrographs of diabase from Site 1117. 1. Undeformed coarse-grained gabbro. Note the development of chlorite patches replacing clinopyroxene (plane-polarized transmitted light). 2. Porphyroclast of zoned amphibole with a brown Mg-Hbl core and a green actinolitic rim. The development of amphibole is associated with the presence of biotite replacing clinopyroxene (plane-polarized transmitted light). 3. Symplectitic texture at the contact between clinopyroxene and plagioclase (plane-polarized transmitted light). 4. Deformed gabbro. Note the development of ductile shear zone consisting of recrystallized quartz in the middle of a cataclasite. The cataclasite zone is made of clinopyroxene, amphibole, and plagioclase grains in a dark brown matrix (plane-polarized transmitted light). 5. Deformed coarse-grained gabbro. Note the development of chlorite flakes along shear bands cutting a porphyroclast of amphibole (plane-polarized transmitted light). 6. Veins filled with a quartz + epidote assemblage are filled with chlorite cutting the brecciated gabbro (cross-polarized transmitted light). Cpx = clinopyroxene, Plg = plagioclase, Glau = glaucony, Chl = chlorite, Qtz = quartz, Ilm = ilmenite, Bio = biotite, Epi = epidote, Hbl = hornblende, Act-Hbl = actinolitic hornblende, Mg-hbl = magnesiohornblende, S = symplectite, Catc = cataclasite.



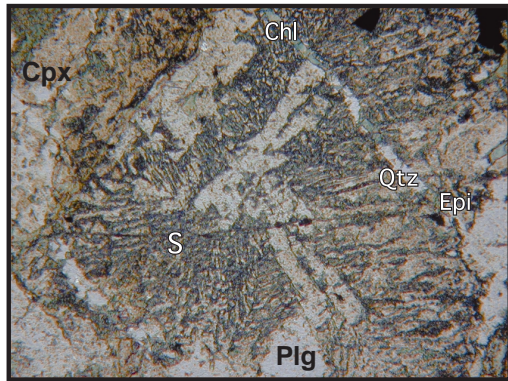
1

2 mm



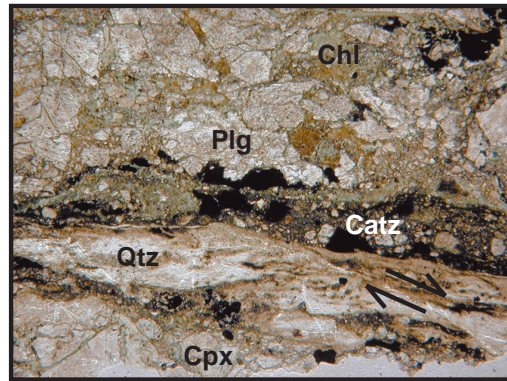
2

2 mm



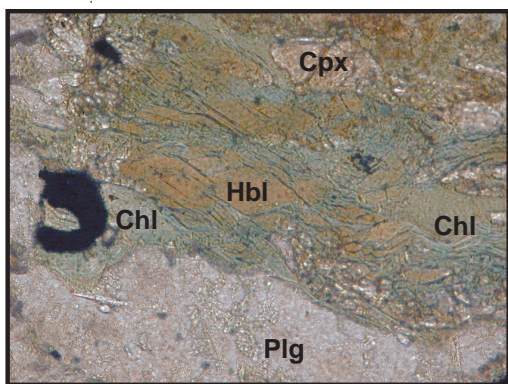
3

2 mm



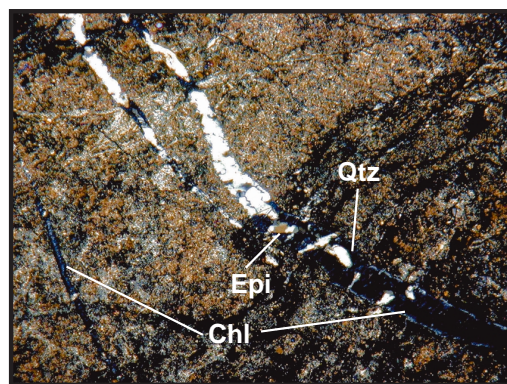
4

2 mm



5

2 mm



6

2 mm